

Improved Search for a Light Sterile Neutrino with the Full Configuration of the Daya Bay Experiment

F. P. An,¹ A. B. Balantekin,² H. R. Band,³ M. Bishai,⁴ S. Blyth,^{5,6} D. Cao,⁷ G. F. Cao,⁸ J. Cao,⁸ W. R. Cen,⁸ Y. L. Chan,⁹ J. F. Chang,⁸ L. C. Chang,¹⁰ Y. Chang,⁶ H. S. Chen,⁸ Q. Y. Chen,¹¹ S. M. Chen,¹² Y. X. Chen,¹³ Y. Chen,¹⁴ J.-H. Cheng,¹⁰ J. Cheng,¹¹ Y. P. Cheng,⁸ Z. K. Cheng,¹⁵ J. J. Cherwinka,² M. C. Chu,⁹ A. Chukanov,¹⁶ J. P. Cummings,¹⁷ J. de Arcos,¹⁸ Z. Y. Deng,⁸ X. F. Ding,⁸ Y. Y. Ding,⁸ M. V. Diwan,⁴ M. Dolgareva,¹⁶ J. Dove,¹⁹ D. A. Dwyer,²⁰ W. R. Edwards,²⁰ R. Gill,⁴ M. Gonchar,¹⁶ G. H. Gong,¹² H. Gong,¹² M. Grassi,⁸ W. Q. Gu,²¹ M. Y. Guan,⁸ L. Guo,¹² R. P. Guo,⁸ X. H. Guo,²² Z. Guo,¹² R. W. Hackenburg,⁴ R. Han,¹³ S. Hans,^{4,*} M. He,⁸ K. M. Heeger,³ Y. K. Heng,⁸ A. Higuera,²³ Y. K. Hor,²⁴ Y. B. Hsiung,⁵ B. Z. Hu,⁵ T. Hu,⁸ W. Hu,⁸ E. C. Huang,¹⁹ H. X. Huang,²⁵ X. T. Huang,¹¹ P. Huber,²⁴ W. Huo,²⁶ G. Hussain,¹² D. E. Jaffe,⁴ P. Jaffke,²⁴ K. L. Jen,¹⁰ S. Jetter,⁸ X. P. Ji,^{27,12} X. L. Ji,⁸ J. B. Jiao,¹¹ R. A. Johnson,²⁸ J. Joshi,⁴ L. Kang,²⁹ S. H. Kettell,⁴ S. Kohn,³⁰ M. Kramer,^{20,30} K. K. Kwan,⁹ M. W. Kwok,⁹ T. Kwok,³¹ T. J. Langford,³ K. Lau,²³ L. Lebanowski,¹² J. Lee,²⁰ J. H. C. Lee,³¹ R. T. Lei,²⁹ R. Leitner,³² J. K. C. Leung,³¹ C. Li,¹¹ D. J. Li,²⁶ F. Li,⁸ G. S. Li,²¹ Q. J. Li,⁸ S. Li,²⁹ S. C. Li,^{31,24} W. D. Li,⁸ X. N. Li,⁸ Y. F. Li,⁸ Z. B. Li,¹⁵ H. Liang,²⁶ C. J. Lin,²⁰ G. L. Lin,¹⁰ S. Lin,²⁹ S. K. Lin,²³ Y.-C. Lin,⁵ J. J. Ling,¹⁵ J. M. Link,²⁴ L. Littenberg,⁴ B. R. Littlejohn,¹⁸ D. W. Liu,²³ J. L. Liu,²¹ J. C. Liu,⁸ C. W. Loh,⁷ C. Lu,³³ H. Q. Lu,⁸ J. S. Lu,⁸ K. B. Luk,^{30,20} Z. Lv,³⁴ Q. M. Ma,⁸ X. Y. Ma,⁸ X. B. Ma,¹³ Y. Q. Ma,⁸ Y. Malyskin,³⁵ D. A. Martinez Caicedo,¹⁸ K. T. McDonald,³³ R. D. McKeown,^{36,37} I. Mitchell,²³ M. Mooney,⁴ Y. Nakajima,²⁰ J. Napolitano,³⁸ D. Naumov,¹⁶ E. Naumova,¹⁶ H. Y. Ngai,³¹ Z. Ning,⁸ J. P. Ochoa-Ricoux,³⁵ A. Olshevskiy,¹⁶ H.-R. Pan,⁵ J. Park,²⁴ S. Patton,²⁰ V. Pec,³² J. C. Peng,¹⁹ L. Pinsky,²³ C. S. J. Pun,³¹ F. Z. Qi,⁸ M. Qi,⁷ X. Qian,⁴ N. Raper,³⁹ J. Ren,²⁵ R. Rosero,⁴ B. Roskovec,³² X. C. Ruan,²⁵ H. Steiner,^{30,20} G. X. Sun,⁸ J. L. Sun,⁴⁰ W. Tang,⁴ D. Taychenachev,¹⁶ K. Treskov,¹⁶ K. V. Tsang,²⁰ C. E. Tull,²⁰ N. Viaux,³⁵ B. Viren,⁴ V. Vorobel,³² C. H. Wang,⁶ M. Wang,¹¹ N. Y. Wang,²² R. G. Wang,⁸ W. Wang,^{37,15} X. Wang,⁴¹ Y. F. Wang,⁸ Z. Wang,¹² Z. Wang,⁸ Z. M. Wang,⁸ H. Y. Wei,¹² L. J. Wen,⁸ K. Whisnant,⁴² C. G. White,¹⁸ L. Whitehead,²³ T. Wise,² H. L. H. Wong,^{30,20} S. C. F. Wong,¹⁵ E. Worcester,⁴ C.-H. Wu,¹⁰ Q. Wu,¹¹ W. J. Wu,⁸ D. M. Xia,⁴³ J. K. Xia,⁸ Z. Z. Xing,⁸ J. Y. Xu,⁹ J. L. Xu,⁸ Y. Xu,¹⁵ T. Xue,¹² C. G. Yang,⁸ H. Yang,⁷ L. Yang,²⁹ M. S. Yang,⁸ M. T. Yang,¹¹ M. Ye,⁸ Z. Ye,²³ M. Yeh,⁴ B. L. Young,⁴² Z. Y. Yu,⁸ S. Zeng,⁸ L. Zhan,⁸ C. Zhang,⁴ H. H. Zhang,¹⁵ J. W. Zhang,⁸ Q. M. Zhang,³⁴ X. T. Zhang,⁸ Y. M. Zhang,¹² Y. X. Zhang,⁴⁰ Y. M. Zhang,¹⁵ Z. J. Zhang,²⁹ Z. Y. Zhang,⁸ Z. P. Zhang,²⁶ J. Zhao,⁸ Q. W. Zhao,⁸ Y. B. Zhao,⁸ W. L. Zhong,⁸ L. Zhou,⁸ N. Zhou,²⁶ H. L. Zhuang,⁸ and J. H. Zou⁸

(Daya Bay Collaboration)

¹*Institute of Modern Physics, East China University of Science and Technology, Shanghai*

²*University of Wisconsin, Madison, Wisconsin USA*

³*Department of Physics, Yale University, New Haven, Connecticut USA*

⁴*Brookhaven National Laboratory, Upton, New York USA*

⁵*Department of Physics, National Taiwan University, Taipei*

⁶*National United University, Miao-Li*

⁷*Nanjing University, Nanjing*

⁸*Institute of High Energy Physics, Beijing*

⁹*Chinese University of Hong Kong, Hong Kong*

¹⁰*Institute of Physics, National Chiao-Tung University, Hsinchu*

¹¹*Shandong University, Jinan*

¹²*Department of Engineering Physics, Tsinghua University, Beijing*

¹³*North China Electric Power University, Beijing*

¹⁴*Shenzhen University, Shenzhen*

¹⁵*Sun Yat-Sen (Zhongshan) University, Guangzhou*

¹⁶*Joint Institute for Nuclear Research, Dubna, Moscow Region*

¹⁷*Siena College, Loudonville, New York USA*

¹⁸*Department of Physics, Illinois Institute of Technology, Chicago, Illinois USA*

¹⁹*Department of Physics, University of Illinois at Urbana-Champaign, Urbana, Illinois USA*

²⁰*Lawrence Berkeley National Laboratory, Berkeley, California USA*

²¹*Department of Physics and Astronomy, Shanghai Jiao Tong University, Shanghai Laboratory for Particle Physics and Cosmology, Shanghai*

²²*Beijing Normal University, Beijing*

²³*Department of Physics, University of Houston, Houston, Texas USA*

²⁴*Center for Neutrino Physics, Virginia Tech, Blacksburg, Virginia USA*²⁵*China Institute of Atomic Energy, Beijing*²⁶*University of Science and Technology of China, Hefei*²⁷*School of Physics, Nankai University, Tianjin*²⁸*Department of Physics, University of Cincinnati, Cincinnati, Ohio USA*²⁹*Dongguan University of Technology, Dongguan*³⁰*Department of Physics, University of California, Berkeley, California USA*³¹*Department of Physics, The University of Hong Kong, Pokfulam, Hong Kong*³²*Charles University, Faculty of Mathematics and Physics, Prague, Czech Republic*³³*Joseph Henry Laboratories, Princeton University, Princeton, New Jersey USA*³⁴*Xi'an Jiaotong University, Xi'an*³⁵*Instituto de Física, Pontificia Universidad Católica de Chile, Santiago, Chile*³⁶*California Institute of Technology, Pasadena, California USA*³⁷*College of William and Mary, Williamsburg, Virginia USA*³⁸*Department of Physics, College of Science and Technology, Temple University, Philadelphia, Pennsylvania USA*³⁹*Department of Physics, Applied Physics, and Astronomy, Rensselaer Polytechnic Institute, Troy, New York USA*⁴⁰*China General Nuclear Power Group, Shenzhen*⁴¹*College of Electronic Science and Engineering, National University of Defense Technology, Changsha*⁴²*Iowa State University, Ames, Iowa USA*⁴³*Chongqing University, Chongqing*

(Received 6 July 2016; published 7 October 2016)

This Letter reports an improved search for light sterile neutrino mixing in the electron antineutrino disappearance channel with the full configuration of the Daya Bay Reactor Neutrino Experiment. With an additional 404 days of data collected in eight antineutrino detectors, this search benefits from 3.6 times the statistics available to the previous publication, as well as from improvements in energy calibration and background reduction. A relative comparison of the rate and energy spectrum of reactor antineutrinos in the three experimental halls yields no evidence of sterile neutrino mixing in the $2 \times 10^{-4} \lesssim |\Delta m_{41}^2| \lesssim 0.3 \text{ eV}^2$ mass range. The resulting limits on $\sin^2 2\theta_{14}$ are improved by approximately a factor of 2 over previous results and constitute the most stringent constraints to date in the $|\Delta m_{41}^2| \lesssim 0.2 \text{ eV}^2$ region.

DOI: 10.1103/PhysRevLett.117.151802

The three-neutrino mixing framework, in which the flavor eigenstates (ν_e, ν_μ, ν_τ) mix with the mass eigenstates (ν_1, ν_2, ν_3) via the Pontecorvo-Maki-Nakagawa-Sakata matrix [1–3], has been extremely successful in explaining the results observed in most solar, atmospheric, reactor, and long-baseline accelerator neutrino oscillation experiments [4]. Despite this success, the exact mechanism by which neutrinos acquire their mass remains unknown, and the possible existence of additional neutrinos is under active consideration. To be consistent with precision electroweak measurements [5], these additional neutrinos are called “sterile” [2], that is, noninteracting within the standard model and thus with no known mechanism for direct detection. Nonetheless, an unambiguous signal of their existence can be sought in neutrino oscillation experiments, where they could affect the way in which the three active neutrinos oscillate if they mix with the latter.

In the simplest extension of the standard model, where only one sterile neutrino is considered in addition to the three active ones, the mixing can be expressed as

$$\nu_\alpha = \sum_{i=1}^4 U_{\alpha i} \nu_i, \quad (1)$$

where U is a unitary 4×4 mixing matrix and $U_{\alpha i}$ is the neutrino mixing matrix element for the flavor eigenstate ν_α and the mass eigenstate ν_i . The survival probability for a relativistic ν_α with an energy E and a traveling distance L is given by

$$P_{\nu_\alpha \rightarrow \nu_\alpha} = 1 - 4 \sum_{i=1}^3 \sum_{j>i}^4 |U_{\alpha i}|^2 |U_{\alpha j}|^2 \sin^2 \Delta_{ji}, \quad (2)$$

where $\Delta_{ji} = 1.267 \Delta m_{ji}^2 (\text{eV}^2) [L(\text{m})/E(\text{MeV})]$ and $\Delta m_{ji}^2 = m_j^2 - m_i^2$ is the mass-squared difference between the mass eigenstates ν_j and ν_i . As indicated in Ref. [6], in the case of electron antineutrino disappearance the neutrino mixing matrix elements U_{ei} can be parametrized in terms of the θ_{14} , θ_{13} , and θ_{12} mixing angles. Compared with standard three-neutrino mixing, the neutrino oscillation probability includes three additional oscillation frequencies associated with Δm_{41}^2 , Δm_{42}^2 , and Δm_{43}^2 . When $|\Delta m_{41}^2| \gg |\Delta m_{31}^2|$ these three parameters are virtually indistinguishable, and for the Daya Bay baselines Eq. (2) approximates to

$$\begin{aligned} P_{\bar{\nu}_e \rightarrow \bar{\nu}_e} &\approx 1 - 4(1 - |U_{e4}|^2) |U_{e4}|^2 \sin^2 \Delta_{41} \\ &\quad - 4(1 - |U_{e3}|^2 - |U_{e4}|^2) |U_{e3}|^2 \sin^2 \Delta_{31} \\ &\approx 1 - \sin^2 2\theta_{14} \sin^2 \Delta_{41} - \sin^2 2\theta_{13} \sin^2 \Delta_{31}. \end{aligned} \quad (3)$$

Thus, to first order, evidence for light sterile neutrino mixing consists of an additional spectral distortion with a frequency different from standard three-neutrino oscillations.

No conclusive evidence for the existence of sterile neutrinos has been obtained. A few anomalies in short baseline neutrino oscillation experiments [7–13] can be explained with additional sterile neutrinos, but these results are in tension with the limits obtained from other experiments [14–17]. The majority of experimental searches have centered on mass-squared differences around 1 eV^2 and higher, whereas the Daya Bay and other medium baseline reactor antineutrino experiments can make unique contributions in the sub-eV scale [6,18–25]. In 2014, the Daya Bay Collaboration reported on a search for light sterile neutrino mixing based on the first 217 days of data acquired with a partial configuration of six functionally identical antineutrino detectors (ADs) deployed at three experimental halls (EHs), the results of which excluded a large, previously unexplored region of parameter space in the $3 \times 10^{-4} \lesssim |\Delta m_{41}^2| \lesssim 0.1 \text{ eV}^2$ range [26]. In this partial configuration, three ADs were installed in two near halls (two in EH1 and one in EH2) and another three in a far hall (EH3). This Letter reports on an improved search made with the full eight-detector configuration shown in Fig. 1 that resulted from the installation of two additional ADs, one in EH2 and another in EH3, in the summer of 2012. The additional 404 days of eight-detector data collected from October 2012 to November 2013 amount to a 3.6 times increase in statistics.

Each AD is a three-zone cylindrical detector composed of two nested acrylic vessels within a concentric stainless steel vessel. The central vessel is filled with 20 tons of gadolinium-doped liquid scintillator (Gd-LS) that serves as

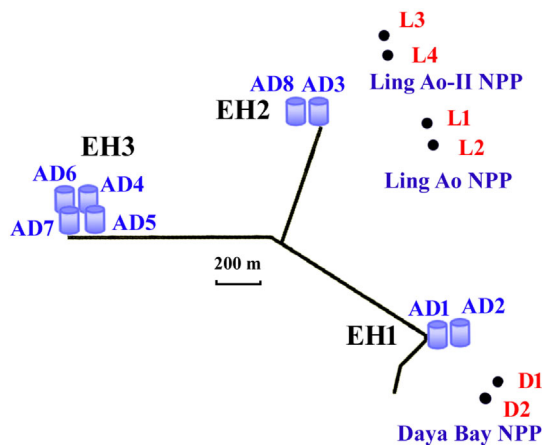


FIG. 1. Layout of the Daya Bay Reactor Neutrino Experiment. The dots represent reactor cores, labeled as D1, D2, L1, L2, L3, and L4. The Daya Bay experiment started data taking with six antineutrino detectors (AD1–AD6) installed in three experimental halls (EH1–EH3). From August to October 2012, two additional detectors (AD7 and AD8) were installed in EH3 and EH2, respectively.

the primary target for antineutrino detection. A 22-ton pure LS volume encloses the central target and enables the detection of γ rays that escape from the Gd LS volume. The outermost cylinder contains 40 tons of mineral oil that provide shielding against γ -ray radiation from the detector components. A total of 192 photomultiplier tubes are installed on the vertical surfaces, and the top and bottom surfaces are covered with optical reflectors. Three automated calibration units [27] that store and deploy calibration sources and Light Emitting Diodes sit on top of the stainless steel vessel. The ADs are housed inside a muon veto system consisting of two optically separated inner and outer water pools [28] that provide shielding from ambient radiation and serve as active water Cherenkov muon detectors. Four layers of resistive plate chambers are installed on top of each water pool. More information on the Daya Bay detectors and their performance can be found in Refs. [29,30].

Reactor antineutrinos are detected via the inverse beta decay (IBD) reaction $\bar{\nu}_e + p \rightarrow e^+ + n$. The positron deposits its energy in the scintillator and then annihilates with an electron. This generates a prompt signal that can be measured with a resolution of $\sigma_E/E \sim 8\%$ at 1 MeV and which preserves most of the incident antineutrino’s energy. The neutron is primarily captured by the gadolinium inside the central target, yielding an $\sim 8 \text{ MeV}$ delayed signal. Requiring coincidence of the prompt and delayed signal pair effectively suppresses backgrounds.

A summary of the IBD candidates for the six-AD and eight-AD periods, together with the estimated background levels and the baselines of the three experimental halls to each pair of reactor cores, is shown in Table I. In the eight-AD period the backgrounds amount to only 2% of the total candidate samples in the near and far halls [31]. Two out of three Am-C calibration sources in the automated calibration units on the top of each far AD were removed during the installation of the two additional ADs in the summer of 2012, which reduced the far hall’s Am-C background by a factor of 4 compared to that in the previous publication. This data set also incorporates a reduction in the AD-uncorrelated energy scale uncertainty from 0.35% to 0.2% due to the implementation of better vertex- and time-dependent corrections [31]. This is one of the dominant systematic uncertainties, and is quantified by studying the differences in detector response using various calibration and natural radioactive sources.

The search for sterile neutrino mixing at the Daya Bay Reactor Neutrino Experiment is carried out through a relative comparison of the antineutrino rates and energy spectra at the three experimental halls. The unique configuration of multiple baselines to three pairs of nuclear reactors allows exploration of Δm_{41}^2 spanning more than 3 orders of magnitude. Figure 2 shows the ratios of the observed prompt energy spectra at EH2 and EH3 to the best fit prediction from EH1 in the three-neutrino case. In this

TABLE I. Summary of total number of IBD candidates and backgrounds, and baselines of the three experimental halls to the reactor pairs. Statistical and systematic errors are included.

Site	IBD candidates		Backgrounds		Mean distance to reactor cores (m)		
	(Six ADs)	(Eight ADs)	(Six ADs)	(Eight ADs)	Daya Bay	Ling Ao	Ling Ao-II
EH1	205 135	408 678	4076.6 ± 462.4	7547.9 ± 908.0	365	860	1310
EH2	93 742	383 402	1580.3 ± 147.8	5791.2 ± 586.5	1348	481	529
EH3	41 348	108 907	1878.9 ± 94.6	2105.2 ± 208.1	1909	1537	1542

figure, the data are compared with the four-neutrino mixing scenario assuming $\sin^2 2\theta_{14} = 0.05$ for two representative Δm_{41}^2 values, illustrating that the sensitivity at $\Delta m_{41}^2 = 4 \times 10^{-2} (4 \times 10^{-3}) \text{ eV}^2$ originates primarily from the relative spectral shape comparison between EH1 and EH2 (EH3). The physical size of the Daya Bay reactor cores and detectors as well as the nonuniform distribution of the fission isotopes inside the cores have a negligible impact on the sensitivity.

The two different analysis methods used in the previous search [26] were updated to include the eight-AD data sample. Both methods, referred to as method A and method B, use the full expression in Eq. (2) to predict the neutrino oscillation signatures. The oscillation parameters $\sin^2 2\theta_{14}$, $\sin^2 2\theta_{13}$, and $|\Delta m_{41}^2|$ are set as free variables, while the others are constrained through external measurements: $\sin^2 2\theta_{12} = 0.846 \pm 0.021$, $\Delta m_{21}^2 = (7.53 \pm 0.18) \times 10^{-5} \text{ eV}^2$, and $|\Delta m_{32}^2| = (2.44 \pm 0.06) \times 10^{-3} \text{ eV}^2$ [32]. The normal mass ordering is assumed for both Δm_{31}^2 and Δm_{41}^2 , although this choice has only a marginal impact on the results.

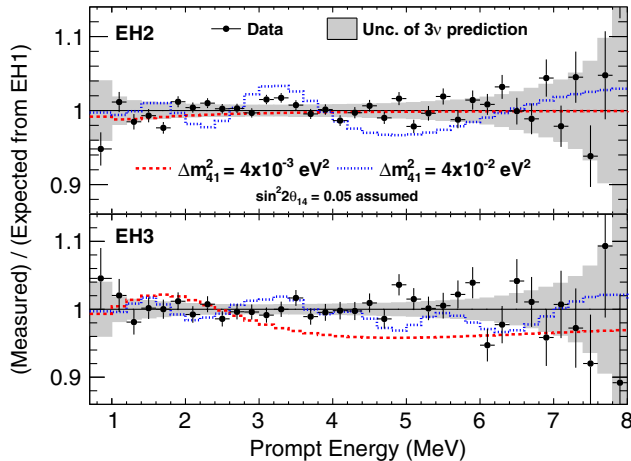


FIG. 2. Prompt energy spectra observed at EH2 (top) and EH3 (bottom), divided by the prediction from EH1 with the three-neutrino best fit oscillation parameters from the most recent Daya Bay analysis [31]. The gray band represents the one-standard-deviation uncertainty of the three-neutrino oscillation prediction, which includes the statistical uncertainty of the EH1 data, as well as all the systematic uncertainties. Predictions with $\sin^2 2\theta_{14} = 0.05$ and two representative Δm_{41}^2 values are also shown as the dotted and dashed curves.

Method A explicitly minimizes the dependence on the reactor antineutrino flux modeling [31] by predicting the prompt energy spectrum at the far hall from the measured spectra at the near halls. This process is done independently for each prompt energy bin i , by applying a weighting factor $w_i(\Delta m_{41}^2, \sin^2 2\theta_{14}, \sin^2 2\theta_{13})$ calculated from the known baselines and the reactor power profiles. The oscillation hypothesis is tested by evaluating a χ^2 defined as

$$\chi^2 = \sum_{i,j} (N_j^f - w_j N_j^n) (V^{-1})_{ij} (N_i^f - w_i N_i^n), \quad (4)$$

where $N_i^{f(n)}$ is the observed number of events after background subtraction in the i th bin at a far (near) detector, and V is a covariance matrix including both systematic and statistical uncertainties. The sensitivity to a spectral distortion between the two near sites is retained by treating their data separately and by having indices i, j run over both the EH3-EH1 and EH3-EH2 combinations. A χ^2 constructed with an alternative combination of the near and far detectors, such as EH2-EH1 and EH3-EH1, yields an equivalent sensitivity. All the sources of systematic error included in the most recent oscillation analysis of Ref. [31] are considered, in addition to the uncertainty in the estimation of Δm_{32}^2 .

Method B simultaneously fits the spectra from all ADs using the predicted reactor antineutrino flux. A binned log-likelihood function is constructed with nuisance parameters for the various systematic terms, including the detector response and the backgrounds. The reactor antineutrino flux is constrained based on the Huber [33] and Mueller [34] fissile antineutrino models. The spectral uncertainties in the models are enlarged as motivated by the observed discrepancy between the predicted reactor antineutrino spectrum and the data [35–38], as well as by the recent reexamination of the systematic uncertainties in Ref. [39]. Specifically, the uncorrelated spectral uncertainties for ^{235}U , ^{239}Pu , and ^{241}Pu are conservatively increased to above 4%, while that of ^{238}U is kept above 10%. The uncertainty of the predicted reactor $\bar{\nu}_e$ rate is also increased to 5%.

The two complementary analysis methods produce practically identical sensitivities for $|\Delta m_{41}^2| \lesssim 0.3 \text{ eV}^2$. Method A is more robust against uncertainties in the

predicted reactor antineutrino flux, while method B has a slightly higher reach in sensitivity for $|\Delta m_{41}^2| \gtrsim 0.3 \text{ eV}^2$ as a result of its incorporation of absolute reactor antineutrino flux constraints. The different treatments of systematic uncertainties provide a thorough cross-check of the results. For method A, the minimum χ^2 value obtained with a free-floating Δm_{41}^2 , $\sin^2 2\theta_{14}$, and $\sin^2 2\theta_{13}$ is $\chi_{4\nu}^2/\text{NDF} = 129.1/145$, where NDF stands for the number of degrees of freedom. The corresponding value in the three-neutrino scenario, in which $\sin^2 2\theta_{13}$ is the only free parameter, is $\chi_{3\nu}^2/\text{NDF} = 134.7/147$. The p -value of observing $\Delta\chi^2 = \chi_{3\nu}^2 - \chi_{4\nu}^2 = 5.6$ without sterile neutrino mixing is determined to be 0.41 using a large sample of Monte Carlo pseudo-experiments. Similarly, the minimum χ^2 values for method B are $\chi_{4\nu}^2/\text{NDF} = 179.74/205$ and $\chi_{3\nu}^2/\text{NDF} = 183.87/207$, with a corresponding p -value of 0.42. As indicated by these p -values, no apparent signature for sterile neutrino mixing is observed.

The limits in the $(|\Delta m_{41}^2|, \sin^2 2\theta_{14})$ plane are also set by two independent approaches, the first of which follows the Feldman-Cousins method [40]. For each point $\boldsymbol{\eta} \equiv (|\Delta m_{41}^2|, \sin^2 2\theta_{14})$, the value of $\Delta\chi^2(\boldsymbol{\eta}) = \chi^2(\boldsymbol{\eta}) - \chi^2(\boldsymbol{\eta}_{\text{best}})$ is evaluated, where $\chi^2(\boldsymbol{\eta})$ is the smallest χ^2 value with a free-floating $\sin^2 2\theta_{13}$. This $\Delta\chi^2(\boldsymbol{\eta})$ is then compared with the critical value $\Delta\chi_c^2(\boldsymbol{\eta})$ encompassing a fraction α of the events, estimated by fitting a large number of pseudo-experiments that include statistical and systematic fluctuations. The point $\boldsymbol{\eta}$ is then declared to be inside the α confidence level (CL) acceptance region if $\Delta\chi_{\text{data}}^2(\boldsymbol{\eta}) < \Delta\chi_c^2(\boldsymbol{\eta})$.

The second approach to set the limits is the CL_s statistical method [41,42]. For each point in the $(\sin^2 2\theta_{14}, |\Delta m_{41}^2|)$ parameter space, a two-hypothesis test is performed in which the null hypothesis H_0 is the three-neutrino model and the alternative hypothesis H_1 is the four-neutrino model with fixed $\sin^2 2\theta_{14}$ and $|\Delta m_{41}^2|$. The CL_s value is defined as

$$\text{CL}_s = \frac{1 - p_1}{1 - p_0}, \quad (5)$$

where p_0 and p_1 are the p -values for the three-neutrino and four-neutrino hypotheses, respectively. These p -values are calculated from the χ^2 difference of those two hypotheses. The value of $\sin^2 2\theta_{13}$ is independently set for each hypothesis based on a fit to the data. The condition of $\text{CL}_s \leq 1 - \alpha$ is required to set the CL_s exclusion region at $[\alpha]$ confidence level.

When used with the same analysis method (method A or method B), the difference in sensitivity between the Feldman-Cousins and CL_s approaches is found to be smaller than 10%. The Feldman-Cousins approach provides a unified method to define confidence intervals, but has the drawback that it involves fitting a large amount of

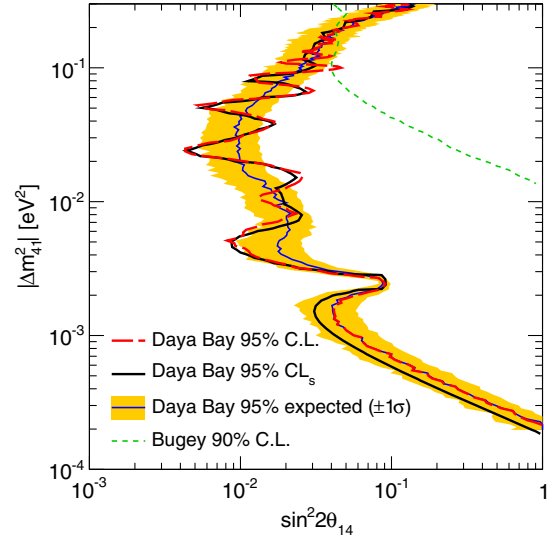


FIG. 3. Exclusion contours in the $(\sin^2 2\theta_{14}, |\Delta m_{41}^2|)$ plane, under the assumption of $\Delta m_{32}^2 > 0$ and $\Delta m_{41}^2 > 0$. The red long-dashed curve represents the 95% CL exclusion contour with the Feldman-Cousins method [40] from method A. The black solid curve represents the 95% CL_s exclusion contour [41] from method B. The expected 95% CL 1σ band in yellow is centered around the sensitivity curve, shown as a thin blue line. The region of parameter space to the right side of the contours is excluded. For comparison, Bugey's [43] 90% CL limit on $\bar{\nu}_e$ disappearance is also shown as the green dashed curve.

simulated data sets. Hence, it is used only for method A, which eliminates all of the nuisance parameters by utilizing a covariance matrix. In contrast, the CL_s implementation is significantly less computationally intensive, and also provides an alternative for combining the results between multiple experiments [41,42]. Accordingly, both the Feldman-Cousins limit from method A and the CL_s limit from method B are presented in this work.

Figure 3 shows the 95% confidence level contour from the Feldman-Cousins approach and the 95% CL_s exclusion contour. Both contours are centered around the 95% CL expectation and are mostly contained within the $\pm 1\sigma$ band constructed from simulated data sets with statistical and systematic fluctuations. The high-precision data at multiple baselines allow exclusion of a large section of $(\sin^2 2\theta_{14}, |\Delta m_{41}^2|)$ parameter space. The sensitivity in the $0.01 \lesssim |\Delta m_{41}^2| \lesssim 0.3 \text{ eV}^2$ region originates predominantly from the relative spectral comparison between the two near halls, and in the $|\Delta m_{41}^2| \lesssim 0.01 \text{ eV}^2$ region from the comparison between the near and far halls. The dip structure at $|\Delta m_{41}^2| \approx |\Delta m_{32}^2| \approx 2.4 \times 10^{-3} \text{ eV}^2$ is due to the degeneracy between $\sin^2 2\theta_{14}$ and $\sin^2 2\theta_{13}$. The fine structure of the data contours compared to the expectation originates from statistical fluctuations in the data.

In Fig. 3, there is a slight difference between the CL contour from method A and the CL_s contour from method B for $|\Delta m_{41}^2| \lesssim 2 \times 10^{-3} \text{ eV}^2$. In this region, most of the

oscillation effects appear in the far hall at prompt energies $\lesssim 2$ MeV, where the statistics are more limited. A study based on a large sample of Monte Carlo pseudo-experiments determined that the two methods react differently to statistical fluctuations and produce slightly different limits in this region. The difference observed in Fig. 3 is found to be consistent with the expectation from this study at the $\sim 1\sigma$ level.

The resulting limits on $\sin^2 2\theta_{14}$ are improved by roughly a factor of 2 compared to the previous publication [26]. The increased statistics are the largest contributor to this improvement, although the reductions in background and in the AD-uncorrelated energy scale uncertainty also play a role. The uncertainty in $|\Delta m_{32}^2|$ is the dominant systematic uncertainty in the $|\Delta m_{41}^2| \lesssim |\Delta m_{32}^2|$ region, while for higher values of $|\Delta m_{41}^2|$ the AD-uncorrelated energy scale and detector efficiency uncertainties are dominant. The total uncertainty is dominated by the statistics; another factor of 2 improvement in sensitivity is expected by 2017. This result can be combined with $\bar{\nu}_\mu \rightarrow \bar{\nu}_e$ disappearance searches [44] in order to constrain $\bar{\nu}_\mu \rightarrow \bar{\nu}_e$ transitions [45], since the oscillation probability of $\bar{\nu}_\mu \rightarrow \bar{\nu}_e$ in the four-neutrino scenario is approximately proportional to $|U_{e4}|^2|U_{\mu 4}|^2$, and the individual sizes of $|U_{e4}|^2$ and $|U_{\mu 4}|^2$ can be constrained with $\bar{\nu}_e$ and $\bar{\nu}_\mu$ disappearance searches, respectively.

In summary, we report an improved search for light sterile neutrino mixing with the full configuration of the Daya Bay Reactor Neutrino Experiment in the electron antineutrino disappearance channel. No evidence of a light sterile neutrino is found through a relative comparison of the observed antineutrino energy spectra at the three experimental halls. With 3.6 times the statistics of the previous publication, these results set the most stringent limits to date on $\sin^2 2\theta_{14}$ in the $2 \times 10^{-4} \lesssim |\Delta m_{41}^2| \lesssim 0.2$ eV² region.

The Daya Bay Reactor Neutrino Experiment is supported in part by the Ministry of Science and Technology of China, the U.S. Department of Energy, the Chinese Academy of Sciences (CAS), the CAS Center for Excellence in Particle Physics, the National Natural Science Foundation of China, the Guangdong provincial government, the Shenzhen municipal government, the China General Nuclear Power Group, the Laboratory Directed Research and Development Program of the Institute of High Energy Physics, the Shanghai Laboratory for Particle Physics and Cosmology, the Research Grants Council of the Hong Kong Special Administrative Region of China, the University Development Fund of the University of Hong Kong, the MOE program for Research of Excellence at National Taiwan University, National Chiao-Tung University, MOST funding support from Taiwan, the U.S. National

Science Foundation, the Alfred P. Sloan Foundation, the Laboratory Directed Research and Development Program of Berkeley National Laboratory and Brookhaven National Laboratory, the Ministry of Education, Youth, and Sports of the Czech Republic, Charles University in Prague, the Joint Institute of Nuclear Research in Dubna, Russia, the NSFC-RFBR joint research program, and the National Commission for Scientific and Technology Research of Chile. We acknowledge the Yellow River Engineering Consulting Co., Ltd., and the China Railway 15th Bureau Group Co., Ltd., for building the underground laboratory. We are grateful for the ongoing cooperation from the China General Nuclear Power Group and China Light and Power Company.

*Present address: Department of Chemistry and Chemical Technology, Bronx Community College, Bronx, New York 10453, USA.

- [1] B. Pontecorvo, *Sov. Phys. JETP* **6**, 429 (1957).
- [2] B. Pontecorvo, *Sov. Phys. JETP* **26**, 984 (1968).
- [3] Z. Maki, M. Nakagawa, and S. Sakata, *Prog. Theor. Phys.* **28**, 870 (1962).
- [4] K. A. Olive *et al.* (Particle Data Group), *Chin. Phys. C* **38**, 090001 (2014).
- [5] S. Schael *et al.* (ALEPH Collaboration, DELPHI Collaboration, L3 Collaboration, OPAL Collaboration, SLD Collaboration, LEP Electroweak Working Group, SLD Electroweak Group, SLD Heavy Flavour Group), *Phys. Rep.* **427**, 257 (2006).
- [6] A. Palazzo, *J. High Energy Phys.* **10** (2013) 172.
- [7] A. Aguilar *et al.* (LSND Collaboration), *Phys. Rev. D* **64**, 112007 (2001).
- [8] A. Aguilar-Arevalo *et al.* (MiniBooNE Collaboration), *Phys. Rev. Lett.* **110**, 161801 (2013).
- [9] A. A. Aguilar-Arevalo *et al.* (MiniBooNE Collaboration), *Phys. Rev. Lett.* **98**, 231801 (2007).
- [10] G. Mention, M. Fechner, T. Lasserre, T. A. Mueller, D. Lhuillier, M. Cribier, and A. Letourneau, *Phys. Rev. D* **83**, 073006 (2011).
- [11] W. Hampel *et al.* (GALLEX Collaboration), *Phys. Lett. B* **420**, 114 (1998).
- [12] J. N. Abdurashitov, V. N. Gavrin, V. V. Gorbachev, P. P. Gurkina, T. V. Ibragimova, A. V. Kalikhov, N. G. Khairnasov, T. V. Knodel, I. N. Mirmov, A. A. Shikhin, E. P. Veretenkin, V. E. Yants, G. T. Zatsepin, T. J. Bowles, S. R. Elliott, W. A. Teasdale, J. S. Nico, B. T. Cleveland, and J. F. Wilkerson (SAGE Collaboration), *Phys. Rev. C* **80**, 015807 (2009).
- [13] C. Giunti and M. Laveder, *Phys. Rev. C* **83**, 065504 (2011).
- [14] G. Karagiorgi, Z. Djurcic, J. M. Conrad, M. H. Shaevitz, and M. Sorel, *Phys. Rev. D* **80**, 073001 (2009).
- [15] J. Kopp, M. Maltoni, and T. Schwetz, *Phys. Rev. Lett.* **107**, 091801 (2011).
- [16] M. Maltoni and T. Schwetz, *Phys. Rev. D* **76**, 093005 (2007).
- [17] S. Gariazzo, C. Giunti, M. Laveder, Y. F. Li, and E. M. Zavanin, *J. Phys. G* **43**, 033001 (2016).
- [18] A. Bandyopadhyay and S. Choubey, [arXiv:0707.2481](https://arxiv.org/abs/0707.2481).

- [19] A. de Gouvea and T. Wytock, *Phys. Rev. D* **79**, 073005 (2009).
- [20] K. Bora, D. Dutta, and P. Ghoshal, *J. High Energy Phys.* **12** (2012) 025.
- [21] S. K. Kang, Y.-D. Kim, Y.-J. Ko, and K. Siyeon, *Adv. High Energy Phys.* **2013**, 138109 (2013).
- [22] P. Bakhti and Y. Farzan, *J. High Energy Phys.* **10** (2013) 200.
- [23] A. Esmaili, E. Kemp, O. L. G. Peres, and Z. Tabrizi, *Phys. Rev. D* **88**, 073012 (2013).
- [24] M. Bergevin, C. Grant, and R. Svoboda, [arXiv:1303.0310](https://arxiv.org/abs/1303.0310).
- [25] I. Girardi, D. Meloni, T. Ohlsson, H. Zhang, and S. Zhou, *J. High Energy Phys.* **08** (2014) 057.
- [26] F. An *et al.* (Daya Bay Collaboration), *Phys. Rev. Lett.* **113**, 141802 (2014).
- [27] J. L. Liu, B. Cai, R. Carr, D. Dwyer, W. Q. Gu, G. S. Li, X. Qian, R. D. McKeown, R. H. Tsang, W. Wang, F. F. Wu, and C. Zhang, *Nucl. Instrum. Methods Phys. Res., Sect. A* **750**, 19 (2014).
- [28] F. P. An *et al.* (Daya Bay Collaboration), *Nucl. Instrum. Methods Phys. Res., Sect. A* **A773**, 8 (2015).
- [29] F. An *et al.* (Daya Bay Collaboration), *Nucl. Instrum. Methods Phys. Res., Sect. A* **685**, 78 (2012).
- [30] F. An *et al.* (Daya Bay Collaboration), *Nucl. Instrum. Methods Phys. Res., Sect. A* **811**, 133 (2016).
- [31] F. An *et al.* (Daya Bay Collaboration), *Phys. Rev. Lett.* **115**, 111802 (2015).
- [32] K. A. Olive *et al.* (Particle Data Group), *Chin. Phys. C* **38**, 090001 (2014).
- [33] P. Huber, *Phys. Rev. C* **84**, 024617 (2011).
- [34] T. A. Mueller, D. Lhuillier, M. Fallot, A. Letourneau, S. Cormon, L. Fechner, M. Giot, T. Lasserre, J. Martino, G. Mention, A. Porta, and F. Yermia, *Phys. Rev. C* **83**, 054615 (2011).
- [35] F. P. An *et al.* (Daya Bay), *Phys. Rev. Lett.* **116**, 061801 (2016).
- [36] F. P. An *et al.* (Daya Bay Collaboration), [arXiv:1607.05378](https://arxiv.org/abs/1607.05378).
- [37] J. H. Choi *et al.* (RENO Collaboration), *Phys. Rev. Lett.* **116**, 211801 (2016).
- [38] Y. Abe *et al.* (Double Chooz Collaboration), *J. High Energy Phys.* **10** (2014) 086 (2014); **02** (2015) 74(E).
- [39] A. C. Hayes, J. L. Friar, G. T. Garvey, G. Jungman, and G. Jonkmans, *Phys. Rev. Lett.* **112**, 202501 (2014).
- [40] G. J. Feldman and R. D. Cousins, *Phys. Rev. D* **57**, 3873 (1998).
- [41] A. L. Read, *J. Phys. G* **28**, 2693 (2002).
- [42] X. Qian, A. Tan, J. J. Ling, Y. Nakajima, and C. Zhang, *Nucl. Instrum. Methods Phys. Res., Sect. A* **827**, 63 (2016).
- [43] Y. Declais *et al.* (Bugey Collaboration), *Nucl. Phys.* **B434**, 503 (1995).
- [44] P. Adamson *et al.* (MINOS Collaboration), following Letter, *Phys. Rev. Lett.* **117**, 151803 (2016).
- [45] P. Adamson *et al.* (DayaBay and MINOS Collaboration), preceding Letter, *Phys. Rev. Lett.* **117**, 151801 (2016).
- [46] See Supplemental Material at <http://link.aps.org/supplemental/10.1103/PhysRevLett.117.151802>, for χ^2 maps for data and Monte Carlo predictions.